RADIATIVE BIOCONVECTION NANOFLUID SQUEEZING FLOW BETWEEN ROTATING CIRCULAR PLATES: *SEMI-NUMERICAL STUDY WITH THE DTM-PADÉ APPROACH*

A. Zeeshan[1], M. B. Arain[1], M. M. Bhatti[2*], F. Alzahrani[3] and O. Anwar Bég[4]

[1]Department of Mathematics and Statistics, International Islamic University, Islamabad 44000,
Pakistan.

[2]College of Mathematics and Systems Science, Shandong University of Science and Technology,
Qingdao, Shandong, 266590, **_China._**

[3]Department of Mathematics, Faculty of Sciences, King Abdulaziz University, PO Box 80203, Jeddah
21589, **_Saudi Arabia._**

[4]Professor & Director- Multi-Physical Engineering Sciences Group, Aeronautical/Mechanical Engineering, Salford University, School of Science, Engineering & Environment, Manchester, M54WT,
_UK._

*Correspondence: mmbhatti@sdust.edu.cn; mubashirme@yahoo.com

ABSTRACT: Modern biomedical and tribological systems are increasingly deploying combinations of nanofluids and bioconvecting micro-organisms which enable improved control of thermal management. Motivated by these developments, in this study a new mathematical model is developed for the *combined nanofluid bioconvection axisymmetric squeezing flow between rotating circular plates* (an important configuration in, for example, rotating bioreactors and lubrication systems). The Buongiorno two-component nanoscale model is deployed, and swimming gyrotactic microorganisms are considered which do not interact with the nanoparticles. Thermal radiation is also included, and a Rosseland diffusion flux approximation utilized. Appropriate similarity transformations are implemented to transform the nonlinear, coupled partial differential conservation equations for mass, momentum, energy, nanoparticle species and motile micro-organism species under suitable boundary conditions from a cylindrical coordinate system, into a dimensionless nonlinear ordinary differential boundary value problem. An efficient scheme known as Differential Transform Method (DTM) combined with Padé-approximations

is then applied to solve the emerging nonlinear similarity equations. The impact of different non-dimensional parameters i.e. *squeezing Reynolds number, rotational Reynolds number, Prandtl number, thermophoresis parameter, Brownian dynamics parameter, thermal radiation parameter, Schmidt number, bioconvection number and Péclet number* on velocity, temperature, nanoparticle concentration and motile gyrotactic microorganism density number distributions are computed and visualized graphically. The torque effects on both plates, i.e., the lower and the upper plate, are also determined. From the graphical results it is seen that momentum in the squeezing regime is suppressed clearly as the upper disk approaches the lower disk. This inhibits the axial flow and produces axial flow retardation. Similarly, by enhancing the value of squeezing Reynolds number, the tangential velocity distribution also decreases. More rigorous squeezing clearly therefore also inhibits tangential momentum development in the regime and leads to tangential flow deceleration. Tables are also provided for multiple values of flow parameters. The numerical values obtained by DTM-Padé computation show very good agreement with Shooting quadrature. DTM-Padé is shown to be a precise and stable semi-numerical methodology for studying rotating multi-physical flow problems. Radiative heat transfer has an important influence on the transport characteristics. When radiation is neglected different results are obtained. It is important therefore to include radiative flux in models of rotating bioreactors and squeezing lubrication dual disk damper technologies since high temperatures associated with radiative flux can impact significantly on combined nanofluid bioconvection which enables more accurate prediction of actual thermofluidic characteristics. Corrosion and surface degradation effects may therefore be mitigated in designs.

KEYWORDS: *Gyrotactic microorganisms; Nanofluids; Thermal radiation; differential transform method, Padé approximants; circular plates; rotating bioreactors; squeezing tribology; torque.*

1   INTRODUCTION

For many industrial purposes, nanotechnology is being increasingly implemented in the 21st century since nanometer-size materials have unique chemical and physical properties. Nanofluids were pioneered by Choi [1] and constitute base liquids containing stable suspended nanoparticles. Due to the comparatively low thermal conductivity of conventional fluids used for heat transfer uses such as mineral oils, ethylene glycol, and water, nanofluids with relatively high heat conductivities have attracted tremendous interest owing to their substantial thermal enhancement capabilities with minimal chances of pressure drop and agglomeration (clustering). During their experimental study, Eastman *et al*. [2] have

shown that a 60 percent increase in thermal conductivity for a nanofluid composed of water and 5 percent volume fraction of CuO nanoparticles, can be achieved. This is achieved due to the considerable enhancement in surface area absorbing heat owing to nanoparticles which manifests in a global boost in thermal conductivity of the nanofluid colloidal suspension. Other factors such as Brownian dynamics and thermophoresis also contribute to this effect. Xuan and Roetzel [3] examined the nanofluid heat transmission efficiency and derived a primary correlation with two approaches for predicting the convective heat conversion of nanofluids. Two fundamental approaches are popular for analyzing nanofluids- firstly, the standard method of treating the nanofluid as a single-phase fluid (e.g. Tiwari-Das model which neglects a species diffusion conservation equation for nanoparticles, but does allow different types of nanoparticle material to be simulated) and secondly the two-phase model for nanofluids (e.g. Buongiorno's nanoscale model which includes a species conservation equation). Chamkha and Aly [4] used Buongirono's model to study the natural convection flow of nanofluids over a vertical porous disc with magnetic field, wall transpiration, heat generation/absorption, Brownian particle motion and thermophoresis effects. Kahveci [5] studied water-based nanofluid circulation in an inclined cavity using the polynomial differential quadrature method (PDQ). Khan and Pop [6] numerically studied the laminar nanofluid boundary layer flow from an extending sheet. Hamid *et al.* [7] computed the thermo-capillary nanofluid radiative convection boundary layer flow with different nanoparticles. Tripathi *et al.* [8] analyzed the bio-inspired pumping of electro-osmotic nanofluids in a deformable tube with axial electrical field effects.

Bioconvection is a process arising when microorganisms (denser than water) are averaged to swim upwards. Bioconvection relates to the propulsion of swimming micro-organisms, controlled by the response to a particular stimulus (taxis). When for example, gyrotactic microorganisms (for which the taxis is torque) and algae are swimming up, they accumulate in the top fluid layer producing a robust and intense stratification which may be fragile. Studies of *nanofluid bioconvection* are aimed at explaining the combined performance of nanoparticles and micro-organisms in an aqueous medium (base fluid) and require robust mathematical models to simulate the propulsion of the microorganisms, migration of nanoparticles and their manipulation under for example inertial, viscous and buoyancy forces. A diverse spectrum of micro-organisms exists in nature, and different types flourish by responding to different stimuli (taxes) e.g. gravitaxis (or geotaxis which respond to gravity), gyrotaxis (torque-driven), phototaxis (light), oxytaxis (oxygen) etc. A variety of theoretical and computational studies of nanofluid bioconvection transport phenomena have been reported in recent years. Alsaedi *et al.* [9] investigated the

heat and mass transfer characteristics in motile gyrotactic microorganism bioconvection nanofluid flow from a stretching surface. Khan *et al.* [10] studied the two-dimensional flow of boundary layer Burgers bioconvection nanofluid. Waqas *et al.* [11] analyzed second-grade viscoelastic nanofluid flow with motile microorganisms from a stretching surface. Kuznetsov [12] investigated the thermoconvective stability of nanofluids containing gyrotactic microorganisms in a horizontal layer. Bhatti *et al.* [13] scrutinized the hydromagnetic Williamson nanofluid bioconvection flow with the effects of thermal radiation. Nima *et al.* [14] used symbolic Maple 14.0 software to compute the near-wall gyrotactic free-forced bioconvection boundary layer flow with oxygen diffusion in a hybrid fuel cell. Amirsom *et al.* [15] used the Buongiorno model and MATLAB Runge-Kutta- Fehlberg quadrature to compute the bioconvection nanofluid boundary layer flow from a bi-axial stretching sheet with anisotropic momentum slip, thermal jump and mass slip effects, as a simulation of hybrid bio-nano-polymer coating flows. They showed that stronger thermophoresis and Brownian dynamics effects enhances nanoparticle concentration whereas velocity and temperatures are suppressed with stronger stretching rate ratio of the bi-axial sheet. Khaled and Khan [16] investigated the radiative heat transfer effects on magnetohydrodynamic viscoplastic nanofluid gyrotactic bioconvection flow from an accelerated surface with variable viscosity properties, observing a boost in temperature with magnetic field, Brownian motion and thermophoresis effects. Aneja et al. [17] applied a variational finite element method to simulate the electromagnetic nanofluid gyrotactic bioconvection flow in fabrication coating flow of smart bio-nano polymer solar coatings. They showed that Nusselt number is depressed with increasing Brownian motion and thermophoresis parameters whereas Sherwood number (nanoparticle mass transfer rate to the wall) is elevated. Further studies of combined gyrotactic bioconvection nanofluid flows include Zohra *et al.* [18] (on magnetic spin coating of a conical body), Uddin *et al.* [19] (on Falkner-Skan magnetohydrodynamic slip bioconvection nanofluid flow with Chebyshev collocation algorithms) and Bég *et al*. [20] (on non-symmetric slip bioconvective nanofluid flow in a porous microchannel with a deforming upper boundary as a model for bio-nano fuel cells). Sohail *et al*. [21] conducted a second law thermodynamic analysis of viscoelastic nanofluid bioconvection with homogeneous-heterogeneous reactions with improved heat conduction and mass diffusion models over a stretched surface. They reported that entropy generation increases for higher values of radiation parameter and Brinkman number, whereas Bejan number is reduced for the higher values of radiation and magnetic parameters. Vasu *et al*. [22] analysed the hydromagnetic viscoplastic nanofluid gyrotactic bioconvection flow from an unsteady stretching sheet with homotopy and generalized differential quadrature (GDQ) methods. They showed that increasing bioconvection Schmidt number suppresses the micro-organism

concentration whereas increasing bioconvection Péclet number boosts both temperatures and nanoparticle concentrations. Several investigators have also considered rotating disk nanofluid bioconvection flows. Zhang *et al.* [23] studied the three-dimensional nanofluid flow due to rotation of circular plates in the presence of gyrotactic microorganisms with magnetic induction effects, noting that microorganism density number is elevated with larger squeeze Reynolds number where as it is reduced with increasing bioconvection Péclet number. Shehzad *et al.* [24] used Runge–Kutta–Fehlberg quadrature to compute the Maxwell viscoelastic nanofluid bioconvection from a rotating radially-stretching disk with a non-Fourier heat flux and Buongiorno model. They observed that radial flow is suppressed whereas temperatures are elevated with greater thermophoretic, Brownian motion and thermal relaxation time parameters and that micro-organisms mass transfer rate to the disk surface is reduced with greater bioconvection Péclet number. Khan *et al.* [25] derived homotopy solutions for nanofluid bioconvection between two stretchable rotating disks with entropy generation, observing that nanoparticles concentration decreases with greater Lewis number and thermophoresis parameter whereas the motile gyrotactic microorganism density numbers are enhanced with greater Lewis and bioconvection Péclet numbers.

Modern bioreactor systems frequently feature parallel *rotating disk* configurations. Engineers are increasingly exploring the use of bioconvection in such devices [26, 27] which feature Von Karman swirling flows between rotating disks and provide a more ecologically viable design [28]. *Chlorella vulgaris* microalgae are an example of gyrotactic bioconvection micro-organisms that can achieve improved efficiency in such devices. In swirling flows of bioreactors, the velocity and spatial scale of the fluid motions will exceed considerably those associated with the swimming speed and size of an individual cell (micro-organism), resulting in rapid transport of cells and the formation of complex spatial patterns in cell concentration. This achieves the desired improvements [29, 30]. By combining nanoparticles with bioconvection micro-organisms, improvements can be achieved in the volumetric efficiency and power consumption. There is therefore considerable motivation to study *rotating bioconvection nanofluid flows* from both a single rotating disk as elaborated in Bég *et al.* [31] and also in between spinning disks [32]. An immense benefit of such systems is that the nanoparticles do not interfere with the micro-organisms or vice versa. This furnishes two excellent mechanisms for controlling heat, mass and momentum transfer characteristics which serve to improve the efficacy of designs.

A scrutiny of the scientific literature has revealed that, thus far, very little effort has been devoted to investigating the impact of *thermal radiative flux on combined nanofluid of gyrotactic micro-organism*

bioconvection in squeezing flow between a pair of rotating circular disks. In addition to rotating bioreactors such flows also find immediate applications in the production of biodiesels and hydrogen [33], which is an essential sustainable energy source and in microbial water treatment plants. Furthermore, squeezing lubrication dual disk damper technologies may also benefit from combined nanofluid bioconvection which has been shown to reduce corrosion and surface degradation effects [34]. High temperature effects invoke radiative heat transfer [35] and in the present study a Rosseland diffusion flux approximation [36-38] is adopted. Axisymmetric viscous incompressible flow is considered. The nonlinear partial differential conservation equations are derived using a modification of the Navier-Stokes viscous flow model with a combination of the Buongiorno two-component nanoscale model [39] and the Kuznetsov bioconvection model [12]. DTM-Padé simulation which combines the classical Differential Transform Method (DTM) with Padé approximants [40] is employed to solve the transformed ordinary differential boundary value problem examine the flow behavior and to obtain the solutions of the given coupled, highly nonlinear ordinary differential equations (ODE's). The effects of various flow parameters (e.g. squeezing Reynolds number, Brownian dynamic parameter, thermophoresis parameter, radiative parameter) on the velocity profile, temperature gradient, concentration of nanoparticles, and motile microorganism density number distributions are visualized graphically and elaborated in detail.

2. MATHEMATICAL MODEL FOR DUAL ROTATING DISK NANO-BIOCONVECTION SQUEEZE FLOW

The regime under study comprises the axisymmetric, viscous, incompressible flow of a nanofluid film doped with micro-organisms and intercalated between two finite parallel rotating disks. A polar (cylindrical) coordinate system is adopted i.e., (r, θ, z) with associated velocity $\breve{U}$ having components (u, v, w). The disks are separated by a distance $\Gamma(t) \left(= (1 - \alpha t)^{1/2} D \right)$ at a time t. The upper rotating disk moving towards the lower stationary disk with velocity $\Gamma'(t)$ as depicted in **Fig. 1**. Both disks are sustained at a constant temperature (T_0, T_l) and nanoparticle concentration (C_0, C_l). Furthermore, the micro-organism density number at both disks is maintained as (n_l, n_u). No slip conditions are also enforced at both disks. In view of these assumptions, the governing equations for mass and momentum (radial, tangential, and axial) conservation may be presented as follows [46-47]:
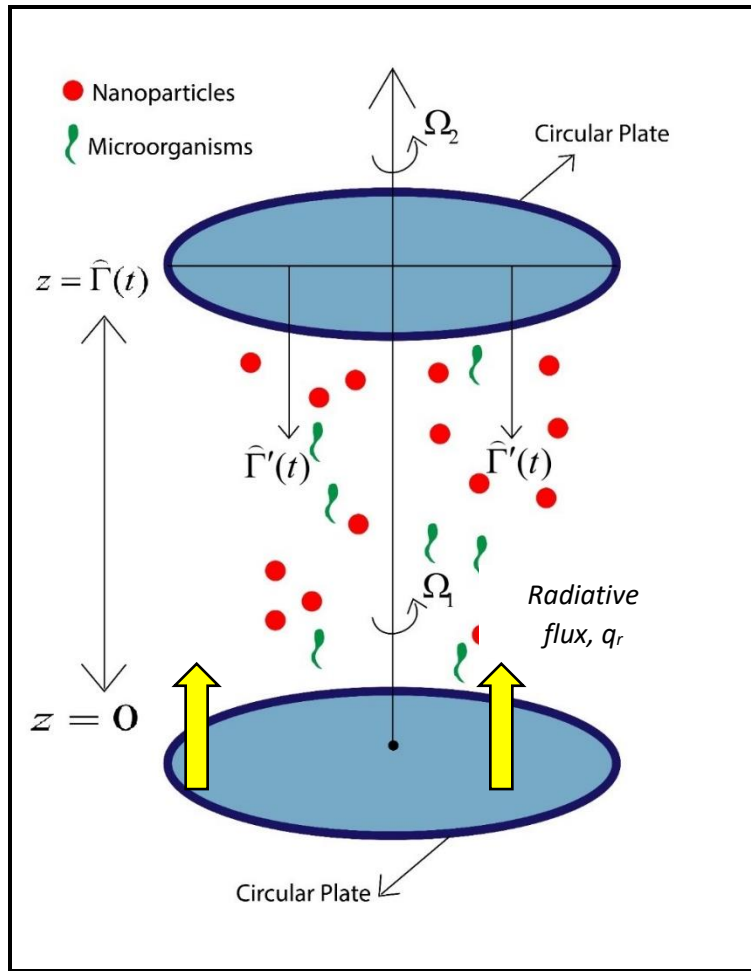
$$\frac{1}{r}\frac{\partial}{\partial r}(rv_r) + \frac{1}{r}\frac{\partial}{\partial \theta}(v_\theta) + \frac{\partial}{\partial z}(v_z) = 0 \tag{1}$$

$$\rho\left(\frac{\partial v_r}{\partial t}+v_r\frac{\partial v_r}{\partial r}+\frac{v_\theta}{r}\frac{\partial v_r}{\partial\theta}+v_z\frac{\partial v_r}{\partial z}-\frac{v_\theta}{r}\right)=-\frac{\partial p}{\partial r}+\mu\left[\frac{1}{r}\frac{\partial v_r}{\partial r}+\frac{1}{r^2}\frac{\partial^2 v_r}{\partial\theta^2}+\frac{\partial^2 v_r}{\partial z^2}-\frac{2}{r}\frac{\partial v_\theta}{\partial\theta}-\frac{v_r}{r^2}\right], \quad (2)$$

$$\rho\left(\frac{\partial v_\theta}{\partial t}+v_r\frac{\partial v_\theta}{\partial r}+\frac{v_\theta}{r}\frac{\partial v_\theta}{\partial\theta}+v_z\frac{\partial v_\theta}{\partial z}-\frac{v_r v_\theta}{r}\right)=-\frac{1}{r}\frac{\partial p}{\partial\theta}+\mu\left[\frac{1}{r}\frac{\partial}{\partial r}\left(r\frac{\partial v_\theta}{\partial r}\right)+\frac{1}{r^2}\frac{\partial^2 v_\theta}{\partial\theta^2}+\frac{\partial^2 v_\theta}{\partial z^2}+\frac{2}{r^2}\frac{\partial v_r}{\partial\theta}-\frac{v_\theta}{r^2}\right], \quad (3)$$

$$\rho\left(\frac{\partial v_z}{\partial t}+v_r\frac{\partial v_z}{\partial r}+\frac{v_\theta}{r}\frac{\partial v_z}{\partial\theta}+v_z\frac{\partial v_z}{\partial z}\right)=-\frac{\partial p}{\partial z}+\mu\left[\frac{1}{r}\frac{\partial}{\partial r}\left(r\frac{\partial v_z}{\partial r}\right)+\frac{1}{r^2}\frac{\partial^2 v_z}{\partial\theta^2}+\frac{\partial^2 v_z}{\partial z^2}\right], \quad (4)$$

Furthermore, ρ, μ, τ denote the nanofluid density, viscosity and stress tensor respectively.

Fig. 1. Geometrical representation of squeezing nanofluid gyrotactic bioconvection between rotating circular disks.

The transport of energy with thermal radiation included may be shown to take the following form [48]:

$$\frac{\partial \breve{T}}{\partial t}+v_r\frac{\partial \breve{T}}{\partial r}+v_z\frac{\partial \breve{T}}{\partial z}-\frac{k}{\rho c_p}\frac{\partial^2 \breve{T}}{\partial z^2}$$

$$+\frac{(\rho c)_p}{(\rho c)_f}\left[D_B\left(\frac{\partial \breve{T}}{\partial r}\frac{\partial \breve{C}}{\partial r}+\frac{\partial \breve{T}}{\partial z}\frac{\partial \breve{C}}{\partial z}\right)+\frac{D_T}{T_\infty}\left[\left(\frac{\partial \breve{T}}{\partial r}\right)^2+\left(\frac{\partial \breve{T}}{\partial z}\right)^2\right]\right]-\frac{1}{(\rho c)_f}\left(\frac{\partial q_r}{\partial r}\right)=0,$$

(5)

Here $\breve{T}$, $\breve{c}$, $\breve{T}_m$, c_p, D_B, D_T and q_r represent temperature, nanoparticle concentration, mean fluid temperature, specific heat at uniform temperature, Brownian diffusivity, thermophoretic diffusion coefficient and radiation heat flux respectively. According to Rosseland approximation radiation heat flux which is uni-directional (acting axially) takes the form, $q_r=-\frac{4\sigma_e}{3\beta_r}\frac{\partial \breve{T}^4}{\partial r}$, in which σ_e represents the Stefan–Boltzmann constant and β_r represents the mean absorption coefficient respectively. Rosseland's model applies for optically thick nanofluids and yields a reasonable estimate for radiative transfer effects although it neglects non-gray effects.

The *nanoparticle concentration conservation* equation reads as follows:

$$\frac{\partial \breve{C}}{\partial t}+v_r\frac{\partial \breve{C}}{\partial r}+v_z\frac{\partial \breve{C}}{\partial z}=D_B\frac{\partial^2 \breve{C}}{\partial z^2}+\frac{D_T}{\breve{T}_u}\frac{\partial^2 \breve{T}}{\partial z^2}.$$

(6)

The *microorganism species conservation equation* takes the form:

$$\frac{\partial n}{\partial t}+v_r\frac{\partial n}{\partial r}+v_\theta\frac{\partial n}{\partial \theta}+v_z\frac{\partial n}{\partial z}+\frac{\bar{b}W_{mo}}{\breve{C}_l-\breve{C}_u}\left[\frac{\partial}{\partial z}\left(n\frac{\partial \breve{C}}{\partial z}\right)\right]=D_{mo}\left(\frac{\partial^2 n}{\partial z^2}\right),$$

(7)

In Eqn. (7), the chemotaxis constant is combined with maximal speed of cell swimming and is denoted by $\bar{b}W_{mo}$ ($\bar{b}W_{mo}$ is considered as a constant) and the diffusivity of micro-organisms is denoted by D_{mo}. The boundary conditions prescribed at the disks which correspond to Eqns. (1-7) are as follows:

$$v_r=0, v_\theta=\Omega_1 r\frac{D^2}{\widehat{\Gamma}^2(t)}, v_z=0, \breve{C}=\breve{C}_l, \breve{T}=\breve{T}_l, n=n_l \quad \text{at} \quad z=0,$$

(8)

$$\begin{cases}v_r=0, v_\theta=\Omega_2 r\frac{D^2}{\widehat{\Gamma}^2(t)}, v_z=-\frac{\alpha D^2}{2\widehat{\Gamma}(t)}, & \text{at} \quad z=\widehat{\Gamma}(t) \\ \breve{T}=\breve{T}_u, \breve{C}=\breve{C}_u, n=n_u,\end{cases}$$

(9)

2.1 Similarity Transformations

The nonlinear partial differential boundary value problem defined by Equations (1)-(7), under boundary conditions (8) and (9) is formidable to solve. It is therefore judicious to render the system dimensionless and the following similarity transformations are therefore invoked:

$$\begin{cases} v_r = r\dfrac{\partial F}{\partial z} = \dfrac{\alpha r}{2}\dfrac{D^2}{\hat{\Gamma}^2(t)}f'(\lambda), \theta = \dfrac{\breve{T}-\breve{T}_u}{\breve{T}_l-\breve{T}_u}, v_\theta = rG(z,t) = r\Omega_1\dfrac{D^2}{\hat{\Gamma}^2(t)}g(\lambda), \\[3mm] v_z = -2F(z,t) = -\dfrac{\alpha D^2 f(\lambda)}{\hat{\Gamma}(t)}, \phi(\lambda) = \dfrac{\breve{C}-\breve{C}_u}{\breve{C}_l-\breve{C}_u}, \chi(\lambda) = \dfrac{n-n_u}{n_l-n_u}, \lambda = \dfrac{z}{\hat{\Gamma}(t)}. \end{cases}$$

(10)

Introducing the similarity transformations (10) in Eqns. (1)-(7), the following nonlinear coupled ordinary differential equations with unit-spaced variable λ (scaled axial coordinate) emerge:

$$f^{(iv)} = S_Q\left[3f'' - 2\left(\dfrac{R_\Omega}{S_Q}\right)^2 gg' - (2f-\lambda)f'''\right],$$

(11)

$$g'' = S_Q\left[2g + \lambda g' + 2gf' - fg'\right],$$

(12)

$$\theta''\left(1+\dfrac{4}{3}R_d\right) + S_Q P_t f\theta' + T_t\theta'^2 + T_b\theta'\phi' = 0,$$

(13)

$$\phi'' + \dfrac{T_t}{T_b}\theta'' + S_Q S_M f\phi' = 0,$$

(14)

$$\chi'' - S_Q B_s\left(\dfrac{\lambda}{2}\right)\chi' + B_s S_Q f\chi' - P_l\left[\chi'\phi' + (\chi+\Phi)\phi''\right] = 0,$$

(15)

In Eqns. (12)-(14) the squeezing Reynolds number is represented by S_Q, rotational Reynolds number is denoted by R_Ω, Brownian motion parameter is represented by T_b, thermophoresis parameter is designated by T_t, Prandtl number is P_t, nanoparticle species Schmidt number is S_M, bioconvection Schmidt number is B_s, and bioconvection Péclet number is Pe, R_d represents the radiation parameter and Φ is a micro-organism bioconvection constant. They are defined as:

$$\begin{cases} S_Q = \dfrac{\alpha D^2}{2\upsilon}, R_\Omega = \dfrac{\Omega_1 D^2}{\upsilon}, T_b = \dfrac{\tau D_B(\breve{C}_l-\breve{C}_u)}{\tilde{\alpha}}, T_t = \dfrac{\tau D_T(\breve{T}_l-\breve{T}_u)}{\tilde{\alpha}\breve{T}_u}, P_t = \dfrac{\upsilon}{\tilde{\alpha}}, S_M = \dfrac{\upsilon}{D_B}, \\[3mm] B_s = \dfrac{\upsilon}{D_n}, P_e = \dfrac{\bar{b}W_{\mathrm{mo}}}{D_{\mathrm{mo}}}, \Phi = \dfrac{n_u}{n_l-u_u}, \alpha = \dfrac{k}{(\rho c_p)_f}, R_d = \dfrac{4\sigma_e\breve{T}_u^3}{\beta_r k}. \end{cases}$$

(16)

The corresponding boundary conditions in Eqns. (8)-(9) are reduced to:

$$\begin{cases} f'(0) = f(0) = 0,\, g(0) = 1,\, \theta(0) = 1,\, \chi(0) = 1,\, \phi(0) = 1, \\ f(1) = \dfrac{1}{2},\, g(1) = \dot{\xi},\, \theta(1) = 0,\, \phi(1) = 0,\, \chi(1) = 0, \end{cases} \tag{17}$$

Here the following notation applies: f represents axial velocity, g represents the tangential velocity, θ represents temperature, ϕ represents nanoparticle concentration, χ is motile microorganism density number. Also $\dot{\xi}\left(= \Omega_2 / \Omega_1\right)$ denotes the angular velocity and the spin velocity range for the dual disk system i.e. for the rotating disks is $-1 \le \dot{\xi} \le 1$; this enables the analysis of different flow scenarios e.g. co-rotating or counter-rotating disks (revolving in the same or opposite directions), of relevance to bioreactor design and also squeezing tribology. Also, of interest in these applications is the *dimensionless torque* on the upper moving disk which is defined as:

$$\dot{T}_{up} = 2\pi\rho \int_0^b \left(D_4 v\right)_{z=\Gamma(t)} dr, \tag{18}$$

Here disk radius is denoted by b. Using Eqn. (10) in Eqn. (18), yields:

$$\dot{T}_{up} = \frac{dg(1)}{d\lambda}, \tag{19}$$

This provides an expression for the non-dimensional torque on the upper moving disk by the swirling nanofluid $(\dot{T}_{up})$ and furthermore the gradient of the tangential velocity on the moving disk is $dg(1)/d\lambda$.

Similarly, the torque in dimensionless form on the lower (fixed) disk is obtained by the same calculation at $\lambda = 0$, giving:

$$\dot{T}_{1p} = \frac{dg(0)}{d\lambda}. \tag{20}$$

3 DTM- PADÉ SOLUTION OF ORDINARY DIFFERENTIAL BOUNDARY VALUE PROBLEM

The 12th order non-linear dimensionless ordinary differential Eqns. (11)-(15) with boundary conditions (17) is solved using a modification of the standard Differential Transform Method (DTM). The DTM produces an analytical result based on Taylor series expansion in polynomial form. Padé approximations aid in increasing the radius of the convergence of the solution of the truncated series. The DTM solutions cannot satisfy the given boundary conditions at $\lambda = 1$ without the use of Padé approximations since, due

to nonlinearity, it is difficult to obtain convergence. It is, therefore, essential to use DTM-Padé simulation to afford an effective way to deal with infinite boundary value problems. This technique has been applied very successfully to address a plethora of multi-physical fluid dynamics problems in the past decade and some relevant works include Bég *et al.* [40] (on electrohydrodynamic ion drag medical pumps), Tripathi *et al.* [41] on non-Newtonian physiological propulsion in the intestinal system, Kumar *et al.* [42] (on thermal couple stress rheological coating flows) and Bhatti *et al.* [43] (on hydromagnetic non-Newtonian boundary layer flows with Hall and Ion slip effects). *MATHEMATICA* symbolic software has been used to evaluate the DTM-Padé approximations. Applying differential transforms to Eqns. (11)-(15), we get:

$$
\begin{aligned}
f(p+4) = \frac{S_Q}{(3+p)(p+2)(4+p)(1+p)} & \Big[3(2+p)(p+1)f(2+p) \\
& + \sum_{i=0}^{q} \Big[(-i+p+1)(-i+2+p)(p+3-i)f(3+p-i)\varepsilon(i) \Big] \\
& - \sum_{i=0}^{q} \Big[2(1-i+p)(p-i+2)(p-i+3)f(i)f(-i+p+3) \Big] \\
& - 2\frac{R_\Omega^2}{S_Q^2} \sum_{i=0}^{q} \Big[(p-i+1)g(i)g(-i+p+1) \Big],
\end{aligned}
\tag{21}
$$

$$
\begin{aligned}
g(p+2) = \frac{S_Q}{(p+2)(1+p)} & \Bigg[2g(p) + \sum_{i=0}^{q} \Big[(1-i+p)+\varepsilon(i)g(-i+1+p) \Big] \\
& + \sum_{i=0}^{q} \Big[2(-i+1+p)g(i)f(1-i+p) - (1+p-i)g(p-i+1)f(i) \Big],
\end{aligned}
\tag{22}
$$

$$
\begin{aligned}
\theta(p+2) = \frac{1}{(p+1)\left(1+\frac{4}{3}R_d\right)(p+2)} & \Bigg[-P_t S_Q \sum_{i=0}^{q} (1+p-i)f(i)\theta(p+1-i) \\
& - \sum_{i=0}^{q} T_t (1+i)(1-i+p)\theta(i+1)\theta(p-i+1) \\
& - \sum_{i=0}^{p} T_b (1+i)(1+p-i)\phi(1-i+q)\theta(i+1) \Bigg],
\end{aligned}
\tag{23}
$$

$$
\phi(p+2) = \frac{1}{(2+p)(1+p)} \left[\begin{array}{l} -S_Q S_M \sum_{i=0}^{q} (p-i+1)\phi(1-i+p)f(i) - \\[2mm] \left(\frac{T_t}{T_b}\right)\theta(2+p)(2+p)(p+1) \end{array} \right],
\tag{24}
$$

$$\chi(p+2) = \frac{1}{(2+p)(1+p)} \left[S_Q S_M \sum_{i=0}^{q} \frac{\varepsilon(i)}{2}(p-i+1)\chi(-i+1+p) \right.$$

$$- S_Q S_M \sum_{i=0}^{q}(-i+1+p)f(i)\chi(-i+1+p)$$

$$+ P_l \left[\sum_{i=0}^{q}(1+i)(-r+1+p)\chi(i+1)\phi(p-i+1) \right. \tag{25}$$

$$+ \sum_{i=0}^{q}(p-i+1)(2-i+p)\chi(i)\phi(2+p+i)$$

$$\left. \left. + \left(\chi(i)+\Phi\right)(2+p)(1+p)\phi(2+p) \right] \right],$$

Here the transformed functions of $f(\lambda), g(\lambda), m(\lambda), n(\lambda), \theta(\lambda), \phi(\lambda)$ and $\chi(\lambda)$ are $F(k), G(k), M(k), N(k), \theta(k), \phi(k)$ and $\chi(k)$ respectively and are expressed as follows:

$$f(\lambda) = \sum_{k=0}^{\infty} f(k)\lambda^{k}, \tag{26}$$

$$g(\lambda) = \sum_{k=0}^{\infty} g(k)\lambda^{k}, \tag{27}$$

$$\theta(\lambda) = \sum_{k=0}^{\infty} \theta(k)\lambda^{k}, \tag{28}$$

$$\phi(\lambda) = \sum_{k=0}^{\infty} \phi(k)\lambda^{k}, \tag{29}$$

$$\chi(\lambda) = \sum_{k=0}^{\infty} \chi(k)\lambda^{k}. \tag{30}$$

The associated boundary conditions are:

$$\left. \begin{array}{lllll} f(0) = 0, & f(1) = \dfrac{1}{2}, & g(0) = 1, & \theta(0) = 1, & \phi(0) = 0, \\ \chi(0) = 0, & f(2) = \Pi_1, & f(3) = \Pi_2, & g(1) = \Pi_3, & \theta(1) = \Pi_4, \\ \phi(1) = \Pi_5, & \chi(1) = \Pi_6 \end{array} \right\} \tag{31}$$

Solving Eqns. (21)-(25) with the help of the boundary conditions given in Eq. (31), we obtain the following series solutions:

$$f(\lambda) = \bar{f_1}\lambda^2 + \bar{f_2}\lambda^3 + \bar{f_3}\lambda^4 + \bar{f_4}\lambda^5 + ..., \tag{32}$$

$$g(\lambda) = 1 - \bar{g_1}\lambda + \bar{g_2}\lambda^2 + \bar{g_3}\lambda^3 + \bar{g_4}\lambda^4 + ..., \tag{33}$$

$$\theta(\lambda) = 1 + \bar{\theta_1}\lambda + \bar{\theta_2}\lambda^2 + \bar{\theta_3}\lambda^3 + \bar{\theta_4}\lambda^4 + ..., \tag{34}$$

$$\phi(\lambda) = 1 + \bar{\phi_1}\lambda + \bar{\phi_2}\lambda^2 + \bar{\phi_3}\lambda^3 + \bar{\phi_4}\lambda^4 + ..., \tag{35}$$

$$\chi(\lambda) = 1 + \bar{\chi_1}\lambda + \bar{\chi_2}\lambda^2 + \bar{\chi_3}\lambda^3 + \bar{\chi_4}\lambda^4 + ..., \tag{36}$$

Here $\bar{f_i}, \bar{g_i}, \bar{\theta_i}, \bar{\phi_i}$ and $\bar{\chi_i}$ where $(i = 1,2,3,...)$ are constants. With the aid of *MATHEMATICA* software, the above equations are solved with 30 iterations. However, the desired rate of convergence is not obtained. Some schemes are available to increase the convergence rate. One of the easiest ways to enhance the rate of convergence of the truncated series is the *Padé approximation* utilized in a rational fraction (ratio of two polynomials). Without Padé approximations, the results attained by DTM do not satisfy the boundary condition at infinity. Therefore, by deploying DTM-Padé simulation, the analytic solution obtained by DTM is combined with the Padé approximation, which gives a reasonable convergence rate at $\lambda = 1$. As a result of numerical values to the desired exactness, the number of terms required is determined by the higher approximation of the order. So, we apply the Padé approximation of order $[5 \times 5]$ to Eqns. (32)-(36), the Padé approximants are as follows.

$$f(\lambda) = \frac{1.70053\lambda^2 - 1.44890\lambda^3 + 0.31487\lambda^4 - 0.06248\lambda^5}{1 + 0.01261\lambda - 0.00403\lambda^2 - 0.00040\lambda^3 - 0.00020\lambda^4 + 0.000063\lambda^5}, \tag{37}$$

$$g(\lambda) = \frac{1 - 1.35929\lambda - 0.14544\lambda^2 + 0.36560\lambda^3 + 0.12128\lambda^4 + 0.01785\lambda^5}{1 - 0.35119\lambda - 0.50948\lambda^2 - 0.14511\lambda^3 - 0.01605\lambda^4 + 0.00075\lambda^5}, \tag{38}$$

$$\theta(\lambda) = \frac{1 - 0.80195\lambda - 0.20532\lambda^2 + 0.00583\lambda^3 - 0.00169\lambda^4 + 0.00325\lambda^5}{1 + 0.07466\lambda - 0.02210\lambda^2 + 0.00570\lambda^3 - 0.00616\lambda^4 + 0.00017\lambda^5}, \tag{39}$$

$$\phi(\lambda) = \frac{1 - 0.71280\lambda - 0.58592\lambda^2 + 0.33874\lambda^3 - 0.056254\lambda^4 + 0.02364\lambda^5}{1 + 0.66107\lambda - 0.03568\lambda^2 + 0.02127\lambda^3 - 0.02173\lambda^4 - 0.00312\lambda^5}, \tag{40}$$

$$\chi(\lambda) = \frac{1 - 0.36377\lambda - 0.71281\lambda^2 + 0.16843\lambda^3 - 0.128773\lambda^4 + 0.03811\lambda^5}{1 + 1.07139\lambda + 0.15110\lambda^2 - 0.02106\lambda^3 - 0.02634\lambda^4 - 0.01361\lambda^5}. \tag{41}$$

4. RESULTS AND DISCUSSION

Extensive DTM-Padé computations have been performed with computational software *MATHEMATICA* to investigate the impact of key thermal, bioconvection and nanoscale parameters on the transport characteristics for the dual disk squeezing regime considered. To verify the exactness of the results, we compare our results with the shooting (numerical quadrature) method. The influence squeezing Reynolds number S_Q, rotational Reynolds number R_Ω, Prandtl number P_t, thermophoresis parameter T_t, Brownian motion T_b, thermal radiation parameter R_d, Schmidt number S_M, bioconvection number B_s, and Péclet number Pe on velocity distribution, temperature profile, nanoparticle concentration, and motile microorganism function are visualized in **Figs 2-9**. In **Table 1**, the numerical results for local Nusselt number, local nanoparticle Sherwood number, and motile density number wall gradient are presented. From this table, it is evident that very good agreement is achieved between DTM-Padé simulation and the numerical shooting method. Eqns. (19,20) are used to calculate the effects of torque on the upper fixed and lower moving disk, and the DTM-Padé computations are displayed in **Table 2**.

Table 1 Comparison of $\theta'(0), \phi'(0), \chi'(0)$ for various values $T_t, T_b, P_t, S_Q, S_M, P_l$ by DTM-Padé$[5 \times 5]$ and the numerical Shooting Method.

T_t	T_b	P_t	S_Q	S_M	P_l	$\theta'(0)$ Shooting Method	$\theta'(0)$ DTM-Padé	$\phi'(0)$ Shooting Method	$\phi'(0)$ DTM-Padé	$\chi'(0)$ Shooting Method	$\chi'(0)$ DTM-Padé
0.03	0.01	6.8	0.01	5	0.5	-0.876624	-0.876624	-1.373875	-1.373875	-1.435174	-1.435174
0.06						-0.788046	-0.788046	-2.275155	-2.275155	-1.831637	-1.831637
0.09						-0.706065	-0.706065	-3.648415	-3.648415	-2.438629	-2.438629
0.05	0.1					-0.583239	-0.583239	-1.212212	-1.212212	-1.361695	-1.361695
	0.3					-0.249589	-0.249589	-1.128954	-1.128954	-1.323609	-1.323609
	0.5					-0.095107	-0.095107	-1.094404	-1.094404	-1.307756	-1.307756
	0.1	4				-0.735315	-0.735315	-1.136189	-1.136189	-1.329559	-1.329559
		7				-0.573375	-0.573375	-1.217143	-1.217143	-1.363747	-1.363747
		10				-0.440450	-0.440450	-1.283606	-1.283606	-1.390905	-1.390905

		6.8	0.01			-0.583239	-0.583239	-1.212212	-1.212212	-1.361695	-1.361695
			0.05			-0.596730	-0.596730	-1.220156	-1.220156	-1.363114	-1.363114
			0.10			-0.613646	-0.613646	-1.229987	-1.229987	-1.364822	-1.364822
			0.01	5		-0.583239	-0.583239	-1.212212	-1.212212	-1.361695	-1.361695
				10		-0.582837	-0.582837	-1.216244	-1.216244	-1.363346	-1.363346
				15		-0.582435	-0.582435	-1.220274	-1.220274	-1.364997	-1.364997
				5	0.5	-0.583239	-0.583239	-1.212212	-1.212212	-1.361695	-1.361695
					1.0	-0.583239	-0.583239	-1.212212	-1.212212	-1.772446	-1.772446
					1.5	-0.583239	-0.583239	-1.212212	-1.212212	-2.226726	-2.226726

Table 2. Values of torque at the lower (fixed) and upper (moving) disks.

|	$\dfrac{dg(0)}{d\lambda}$		$\dfrac{dg(1)}{d\lambda}$	
S_Q	DTM-Padé Result	Numerical Result (Shooting Method)	DTM-Padé Result	Numerical Result (Shooting Method)
0.01	-1.008097	-1.008097	-0.991545	-0.995462
0.05	-1.039719	-1.039719	-0.977810	-0.977806
0.10	-1.078561	-1.078561	-0.956358	-0.956359
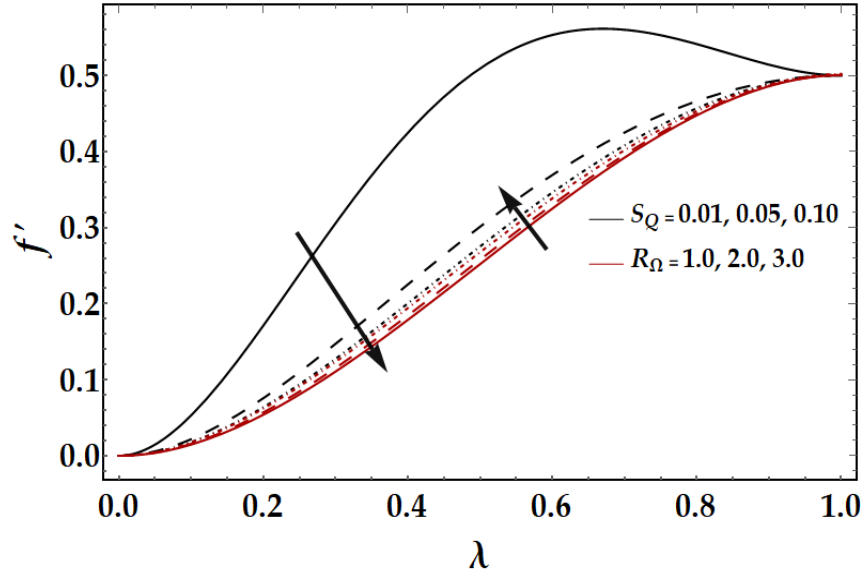
Fig. 2. Influence of various values of squeezing Reynolds number S_Q and rotational Reynolds number R_Ω on velocity distribution (axial) $f'(\lambda)$
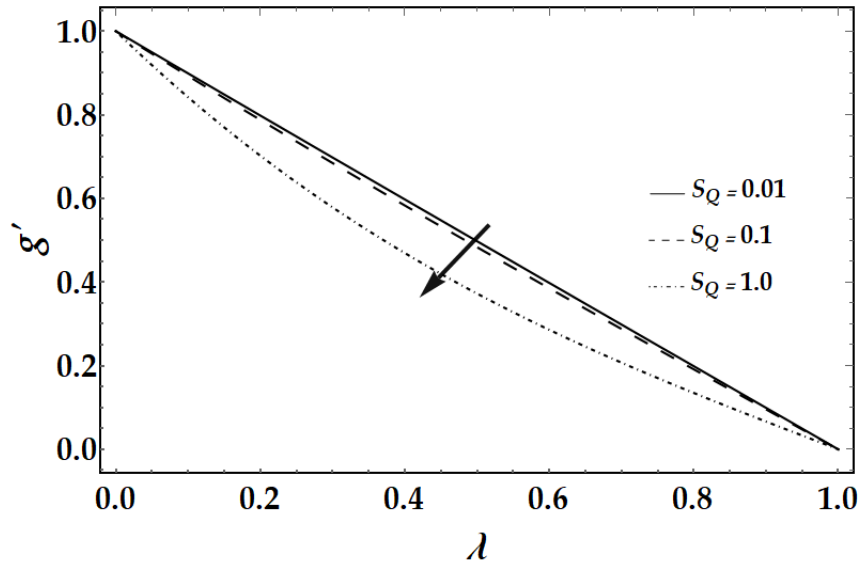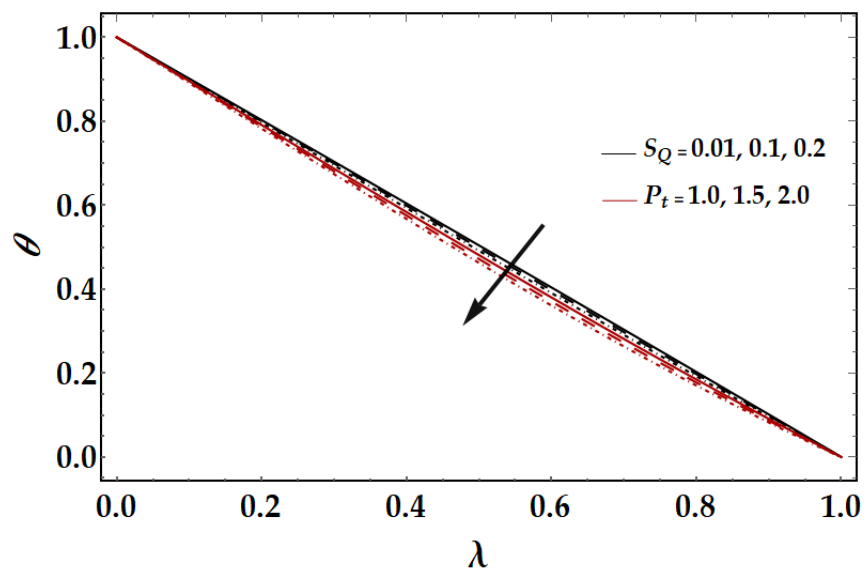

Fig. 3. Influence of various values of squeezing Reynolds number S_Q on the velocity distribution (tangential) $g'(\lambda)$
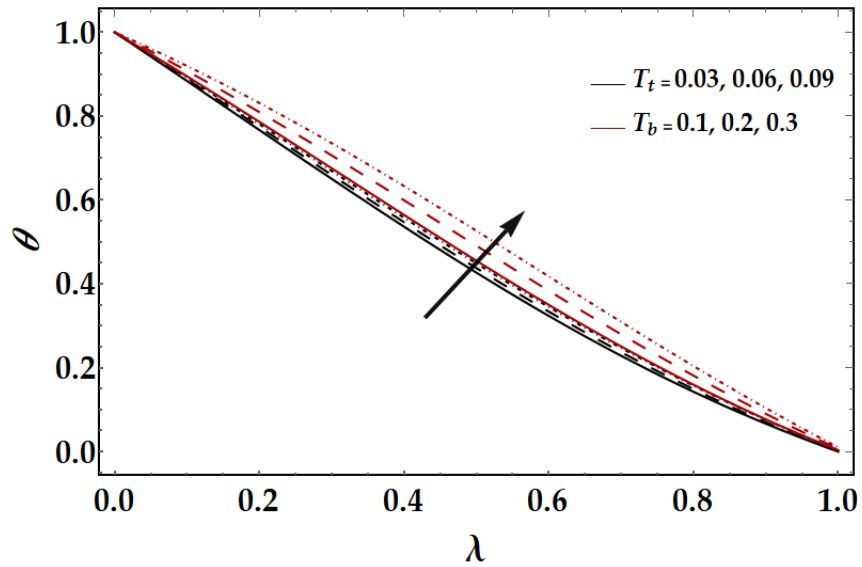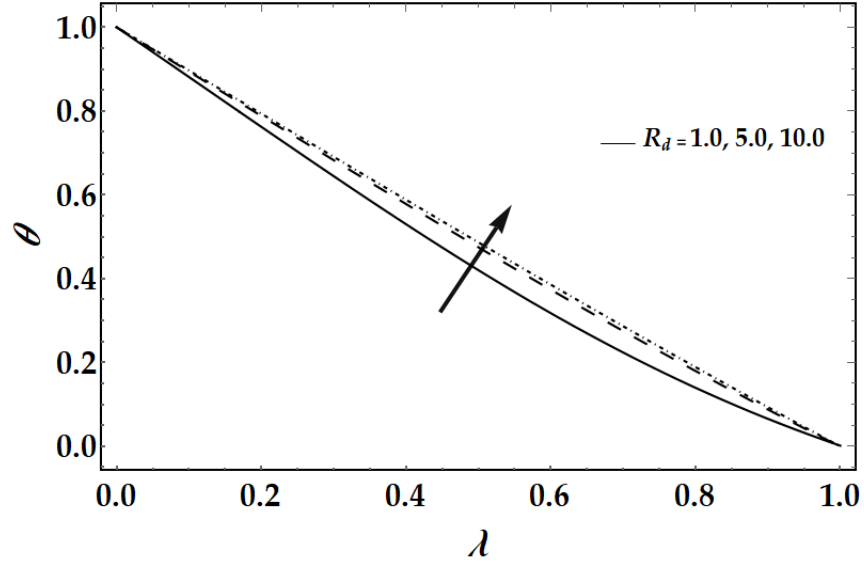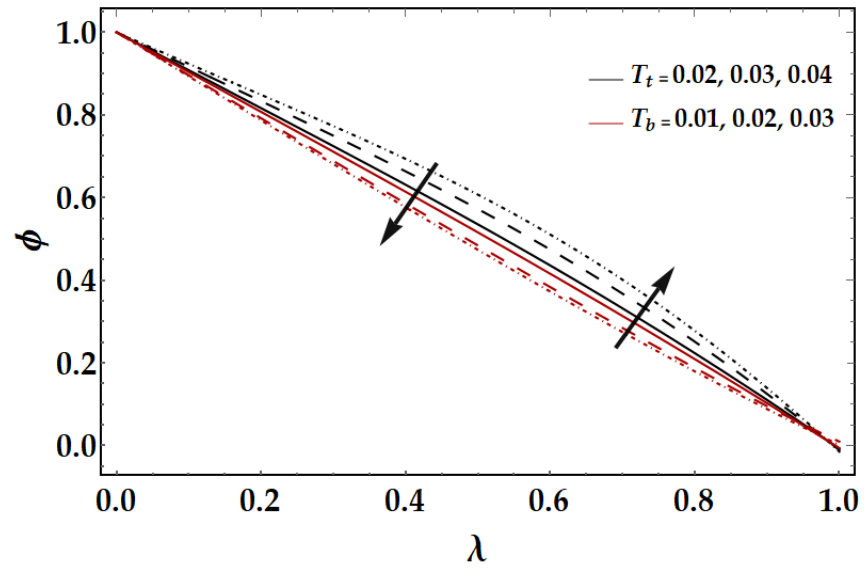
Fig. 4. Influence of various values of thermophoresis parameter T_t and Brownian motion parameter T_b on the temperature distribution $\theta(\lambda)$.
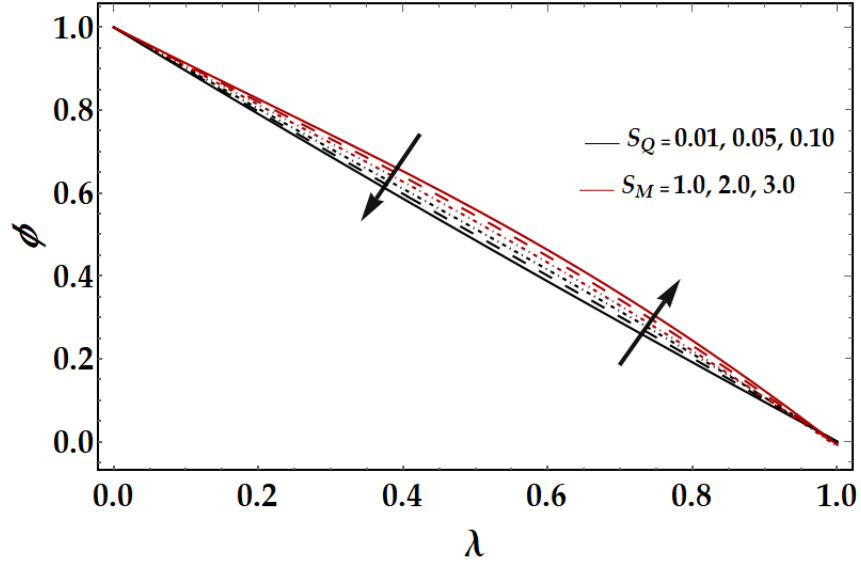

Fig. 5. Influence of various values of squeezing Reynolds number S_Q, Prandtl number P_t on the temperature distribution $\theta(\lambda)$.
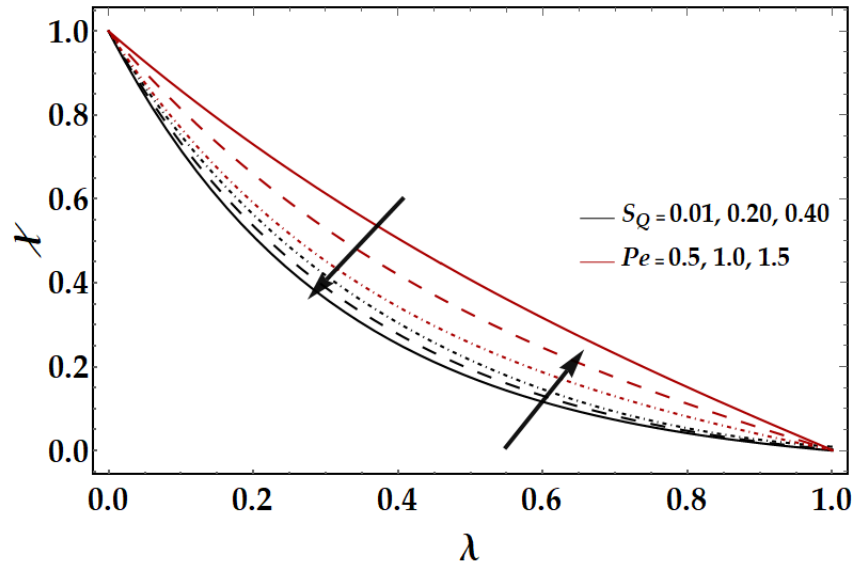
Fig. 6. Influence of different values of radiation parameter R_d on the temperature distribution $\theta(\lambda)$.

Fig. 7. Influence of various values of thermophoresis parameter T_t and Brownian motion parameter T_b on the nanoparticle volume fraction $\phi(\lambda)$.

Fig. 8. Influence of various values of squeezing Reynolds number S_Q, Schmidt number S_M on the nanoparticle volume fraction $\phi(\lambda)$.

Fig. 9. Influence of various values of squeezing Reynolds number S_Q, Péclet number Pe on the motile microorganism density function $\chi(\lambda)$.

In all graphs robust data is extracted for thermal, nanofluid, bioconvection, squeezing and radiative heat flux parameters based on the references [1], [10], [29], [31], [34]. This provides a realistic range for bioreactor and also squeezing rotating bio-nanofluid radiative systems.

Fig. 2 shows the collective impact of squeezing Reynold number S_Q and rotational Reynolds number R_Ω .on the axial velocity distribution $f'(\lambda)$. It is observed that when the values of squeezing Reynolds number S_Q are enhanced, the axial velocity distribution decreases. Momentum in the squeezing regime is suppressed clearly as the upper disk approaches the lower disk. This inhibits the axial flow and produces axial flow retardation. It is also noteworthy that for very low squeezing Reynolds number (S_Q = 0.01), a velocity overshoot (peak) is computed closer to the upper disk (λ=1.0); this feature vanishes with higher S_Q values owing to the *damping effect* induced on the axial flow with more intense squeezing. However, with increasing the values of rotational Reynolds number R_Ω the axial velocity $f'(\lambda)$ is increased, since the rotational inertial force is amplified with greater R_Ω values, relative to the viscous hydrodynamic force. $R_\Omega = \frac{\Omega_1 D^2}{\upsilon}$ and expresses the ratio of these two forces as defined in Eqn. (16). The axial and tangential velocity fields are coupled via the term, $-2\left(\frac{R_\Omega}{S_Q}\right)^2 gg'$, in the axial momentum Eqn. (11) and also via terms, $+2gf' - fg'$, in the tangential momentum Eqn. (12). Both velocity components are either directly or indirectly influenced by Reynolds number. The dominant effect is however an *acceleration in axial flow*.

Fig. 3 shows the impact of squeezing Reynolds (S_Q) number on tangential velocity distribution $g'(\lambda)$. It is evident that by enhancing the value of squeezing Reynolds number, the tangential velocity distribution also decreases. More rigorous squeezing clearly therefore also inhibits tangential momentum development in the regime and leads to tangential flow deceleration. It is also interesting to note (**Fig. 3**) that while the *minimum axial velocity* is computed at the lower disk (λ=0.0) and the maximum at the upper disk (λ=1.0), the reverse behaviour is computed for the tangential velocity. This is explained by the re-distribution in momentum in the swirling squeezing regime which is a characteristic of both classical and modified Von Karman rotating flows, as elaborated by Bég [32]. The maximum tangential velocity corresponds to the lower (stationary) disk and minimal velocity arises at the upper (downward moving) disk. The linear decays in tangential velocity profile between the lower and upper disk for lower squeezing

Reynolds number values (S_Q =0.01, 0.1) are morphed into a parabolic topology at maximum squeezing Reynolds number (S_Q =1.0).

Fig. 4 displays the influence of the thermophoresis parameter T_t and the Brownian motion parameter T_b on the temperature profile $\theta(\lambda)$. The graph illustrates that enhancing the values of the thermophoresis parameter and Brownian motion parameter considerably elevate the temperature magnitudes i.e. heat the squeezing swirling flow regime. The ballistic collisions of the nanoparticles produce an enhancement in the conversion of kinetic energy of the nanoparticles to thermal energy. This is dissipated as heat and temperatures are hiked, as noted by Zohra *et al*. [18]. The presence of rotational body force would also appear to amplify this effect [31]. In all cases approximately linear decays in temperature are computed from the lower disk (maximum) to the upper disk (minimum). The influence of Brownian dynamics is also more pronounced than for thermophoretic body force which encourages the migration of the nanoparticles under a temperature gradient to cooler zones in the regime.

Fig. 5 illustrates the evolution in temperature, $\theta(\lambda)$ with a variation in squeezing Reynolds number, S_Q and Prandtl number P_t. It is observed that increment in the Prandtl number P_t, leads to a depletion in temperature magnitudes. This is attributable to the *depletion* in thermal conductivity with larger Prandtl number (Prandtl number is inversely proportional to thermal conductivity for fixed values of dynamic viscosity and specific heat capacity of the nanofluid) which cools the regime i.e. produces a resulting temperature decline. It is also noted that the temperature profile declines with increasing value of squeezing Reynolds number S_Q. The destruction in axial momentum with greater squeezing also inhibits thermal diffusion in the regime which a produces cooling effect. This is clearly beneficial in lubrication applications and also assists in improved thermal control of the regime in rotating bioreactor design.

Fig. 6 depicts the effects of thermal radiation parameter, R_d on temperature distribution between the two disks. It is observed that an increment in the value of the thermal radiation parameter considerably accentuates the temperature magnitudes. The parameter, R_d, arises in the augmented thermal diffusion term in the energy conservation Eqn. (13), viz $\theta''\left(1 + \frac{4}{3}R_d\right)$. The parameter $R_d = \frac{4\sigma_e \breve{T}_u^3}{\beta_r k}$ simulate the relative role of radiative heat transfer to thermal conduction heat transfer. It is also known as the Boltzmann number or Stark number. When $Rd \rightarrow 0$ radiative flux vanishes. For *Rd =1, both radiative and*

conduction heat flux contribute equally. However, for Rd < 1, thermal conduction is the dominant heat transfer mode and vice versa for Rd > 1. We consider cases where Rd =1, 5, 10 for which the radiative flux becomes very strong and this leads to energization of the nanofluid squeezing regime. Temperatures are therefore boosted significantly. The implication is that when radiative transfer is neglected or small in contribution, in mathematical models, temperatures are under-predicted. Temperatures are therefore boosted significantly since heat transfer is augmented with radiative heat transfer which assists both thermal convection and thermal conduction in the regime. Clearly when radiative flux is neglected, temperatures will be under-predicted which is undesirable in real designs of bioreactors and squeezing lubrication systems. A more accurate determination of temperature field therefore requires the inclusion of radiative transfer models. Of course, the present Rosseland diffusion flux model, only furnishes a *simple* approximation for radiative transfer. It may however be refined to consider more complex behaviour using e.g. the Trauggot P1 differential approximation, which would appear to be quite promising for future studies [44] involving nanofluids. To consider a variation in optical thickness of the nanofluid would require yet more complex models such as the Chandrasekhar discrete ordinates model.

Fig. 7 visualizes the influence of the thermophoresis parameter T_t and the Brownian motion T_b on the nanoparticle concentration $\phi(\lambda)$. It is observed that the concentration of nanoparticles falls with an increment in Brownian motion parameter T_b since ballistic collisions are exacerbated and this inhibits the transport of nanoparticles in the fluent medium. Conversely, the concentration of nanoparticle increases when values of the thermophoresis parameter T_t are elevated. Thermal gradient driving the thermophoretic migration is therefore *beneficial* to the diffusion of nanoparticles whereas the haphazard motion associated with Brownian dynamics impedes nanoparticle migration.

Fig. 8 shows the impact of squeezing Reynolds number S_Q and Schmidt number S_M. By increasing the values of squeezing Reynolds number S_Q, the nanoparticle concentration $\phi(\lambda)$ is boosted, while the opposite behavior is observed with increment in the value of the Schmidt number S_M. Clearly the suppressive effect of enhanced squeezing decreases the volume of the nanofluid film intercalated between the disks. This increases the concentration of nanoparticles since the same quantity of nanoparticles is squeezed into a smaller overall volume. However, with increasing Schmidt number, as defined by $S_M = \frac{\upsilon}{D_B}$ in Eqn. (16), for a fixed dynamic viscosity, there must be a reduction in nanoparticle

mass diffusivity. This manifests in a depletion in the nanoparticle concentration magnitudes as the nanoparticle diffusion rate is reduced.

Fig. 9 portrays the influence of squeezing Reynolds number S_Q and bioconvection Péclet number *Pe* on gyrotactic micro-organism density number function, $\chi(\lambda)$. It is apparent that there is a substantial increment in microorganism density number with the rise in the squeezing Reynolds number S_Q which (as with the case of the nanoparticle species) may be attributed to the significant decrease in volume of nanofluid due to enhanced squeezing. This constrains the same number of micro-organisms in a smaller overall nanofluid film volume and naturally elevates their concentrations (density numbers). On the contrary, elevation in bioconvection Péclet number *Pe* induces the opposite effect- there is a significant reduction in the microorganism density number. As defined in Eqn. (16), bioconvection Péclet number $P_e = \frac{\bar{b}W_{\mathrm{mo}}}{D_{\mathrm{mo}}}$ and is inversely proportional to the species diffusivity of the microorganisms. Larger Pe values (with a fixed product of chemotaxis constant and maximal speed of cell swimming i.e. $\bar{b}W_{\mathrm{mo}}$ is constant) will inevitably result in a reduction in micro-organism diffusivity. This will counteract the propulsion of the gyrotactic micro-organisms and result in a significant suppression in microorganism density number magnitudes.

Finally it is noteworthy from inspection of **Table 2**, that the torque at the lower (fixed) disk $\frac{dg(0)}{d\lambda}$ *i.e. tangential velocity gradient,* and the torque at the upper (moving) disk, $\frac{dg(1)}{d\lambda}$ are respectively *decreased* (i.e. more negative values) and *increased* (i.e. less negative values) with an increase in the squeezing Reynolds number, S_Q . Therefore, while axial momentum is reduced in the squeezing regime (Fig. 2) it has a different impact on the torque at the lower and upper disks. The amplification in squeezing effect reduces torque at the lower disk whereas it enhances torque at the upper disk.

5. CONCLUSIONS

Motivated by emerging applications in nanofluid-bioconvection rotating bioreactors and bio-inspired nanotechnological lubrication systems, in this article, a new mathematical model has been derived for *combined radiative nanofluid gyrotactic microorganisms bioconvection axisymmetric squeezing flow*

between rotating circular disks using the Buongiorno two-component nanoscale model, Kuznetsov bioconvection model and Rosseland diffusion flux model. The upper disk moves downward and the lower disk is fixed translationally, although both diss co-rotate. An efficient scheme known as DTM-Padé simulation which combines the classical differential transform method (DTM) with Padé-approximations has been deployed to solve the emerging nonlinear similarity ordinary differential equation boundary value problem with appropriate no slip and isothermal, iso-nano-solutal and is-micro-organism density number boundary conditions. The Padé approximation with the Differential transform method (DTM) successfully increases the convergence rate whereas at $\lambda = 1$, the DTM does not converge. It is seen that after merging the Differential Transform Method (DTM) with Padé approximants, the results are markedly improved, which is confirmed with close corroboration with a numerical shooting method. Tables are also provided for multiple values of flow parameters, and a comparison is obtained with the shooting method, which shows that DTM-Padé is precise and stable. The main findings of the simulations may be summarized as follows:

i.   With increment in squeezing Reynolds number, both axial and tangential velocity magnitudes decrease.

ii.   By raising the values of the rotational Reynolds number, the axial velocity distribution increases.

iii.   A rise in the values of thermophoresis parameter induces significant elevation in nanoparticle concentration values.

iv.   By Increasing the value of Brownian motion and thermophoresis parameters, fluid temperature is increased due to elevation in the kinetic energy of the nanoparticles.

v.   Thermal conductivity reduces when we increase the value of the Prandtl number which declines the temperature profile.

vi.   Greater thermal radiation parameter energizes the squeezing regime and enhances the temperature distribution. The inclusion of radiative flux therefore produces different results to when it is neglected, and it is important in realistic models of high temperature bioreactors or lubrication systems to include a robust radiative heat transfer model.

vii.   Speed of the microorganism decreases because the microorganism density function decreases while increasing the Péclet number.

viii.   The amplification in squeezing effect i.e., *greater squeezing Reynolds number*, reduces torque at the lower disk whereas it enhances torque at the upper disk.

The present study has demonstrated the excellent accuracy of DTM-Padé simulation in rotating nanofluid bioconvection squeezing flows. However, attention has been restricted to *Newtonian nanofluids*. Future studies may generalize the present analysis to consider non-Newtonian effects (e.g., micropolar fluids [45]) which are also relevant to bioreactor configurations and lubrication regimes and will be communicated imminently.

REFERENCES

[1] Choi SU. Nanofluids: from vision to reality through research. ASME Journal of Heat transfer. 2009;131(3).

[2]   Eastman JA, Choi US, Li S, Thompson LJ, Lee S. Enhanced thermal conductivity through the development of nanofluids. MRS Online Proceedings Library (OPL). 1996;457.

[3]   Xuan Y, Roetzel W. Conceptions for heat transfer correlation of nanofluids. International Journal of heat and Mass transfer. 2000;43(19):3701-7.

[4]   Chamkha AJ, Aly AM. MHD free convection flow of a nanofluid past a vertical plate in the presence of heat generation or absorption effects. Chemical Engineering Communications. 2010;198(3):425-41.

[5]   Kahveci K. Buoyancy driven heat transfer of nanofluids in a tilted enclosure. Journal of Heat Transfer. 2010;132(6).

[6]   Khan WA, Pop I. Boundary-layer flow of a nanofluid past a stretching sheet. International journal of heat and mass transfer. 2010;53(11-12):2477-83.

[7]   Hamid A, Arifin NM, Nazar RM, Pop I. Radiation effects on Marangoni boundary layer flow past a flat plate in nanofluid. InWorld Congress on Engineering 2012. July 4-6, 2012. London, UK. 2010 (Vol. 2189, pp. 1260-1263). International Association of Engineers.

[8]   Tripathi D, Sharma A, Bég OA. Electrothermal transport of nanofluids via peristaltic pumping in a finite micro-channel: Effects of Joule heating and Helmholtz-Smoluchowski velocity. International Journal of Heat and Mass Transfer. 2017;111:138-49.

[9]   Alsaedi A, Khan MI, Farooq M, Gull N, Hayat T. Magnetohydrodynamic (MHD) stratified bioconvective flow of nanofluid due to gyrotactic microorganisms. Advanced Powder Technology. 2017;28(1):288-98.

[10]   Khan M, Irfan M, Khan WA. Impact of nonlinear thermal radiation and gyrotactic microorganisms on the Magneto-Burgers nanofluid. International Journal of Mechanical Sciences. 2017;130:375-82.

[11]   Waqas H, Khan SU, Hassan M, Bhatti MM, Imran M. Analysis on the bioconvection flow of modified second-grade nanofluid containing gyrotactic microorganisms and nanoparticles. Journal of Molecular Liquids. 2019;291:111231.

[12]   Kuznetsov AV. The onset of nanofluid bioconvection in a suspension containing both nanoparticles and gyrotactic microorganisms. International Communications in Heat and Mass Transfer. 2010;37(10):1421-5.

[13]   Waqas H, Khan SU, Imran M, Bhatti MM. Thermally developed Falkner–Skan bioconvection flow of a magnetized nanofluid in the presence of a motile gyrotactic microorganism: Buongiorno's nanofluid model. Physica Scripta. 2019;94(11):115304.

[14] Nima NI, Ferdows M, Anwar Bég O, Kuharat S, Alzahrani F. Biomathematical model for gyrotactic free-forced bioconvection with oxygen diffusion in near-wall transport within a porous medium fuel cell. International Journal of Biomathematics. 2020;13(04):2050026.

[15] Amirsom NA, Uddin MJ, Basir MF, Ismail AI, Beg OA, Kadir A. Three-dimensional bioconvection nanofluid flow from a bi-axial stretching sheet with anisotropic slip. Sains Malaysiana. 2019;48(5):1137-49.

[16] Al-Khaled K, Khan SU. Thermal aspects of Casson nanoliquid with gyrotactic microorganisms, temperature-dependent viscosity, and variable thermal conductivity: bio-technology and thermal applications. Inventions. 2020;5(3):39.

[17] Aneja M, Sharma S, Kuharat S, Anwar Beg O. Computation of electroconductive gyrotactic bioconvection under nonuniform magnetic field: Simulation of smart bio-nanopolymer coatings for solar energy. International Journal of Modern Physics B. 2020:2050028.

[18] Zohra FT, Uddin MJ, Ismail AI, Bég OA, Kadir A. Anisotropic slip magneto-bioconvection flow from a rotating cone to a nanofluid with Stefan blowing effects. Chinese journal of physics. 2018;56(1):432-48.

[19] Uddin MJ, Kabir MN, Bég OA, Alginahi Y. Chebyshev collocation computation of magneto-bioconvection nanofluid flow over a wedge with multiple slips and magnetic induction. Proceedings of the Institution of Mechanical Engineers, Part N: Journal of Nanomaterials, Nanoengineering and Nanosystems. 2018;232(4):109-22.

[20] Bég OA, Basir MF, Uddin MJ, Ismail AM. Numerical study of slip effects on unsteady asymmetric bioconvective nanofluid flow in a porous microchannel with an expanding/contracting upper wall using Buongiorno's model. Journal of Mechanics in Medicine and Biology. 2017;17(03):1750059.

[21] Sohail M, Naz R, Abdelsalam SI. On the onset of entropy generation for a nanofluid with thermal radiation and gyrotactic microorganisms through 3D flows. Physica Scripta. 2020;95(4):045206.

[22] Ray AK, Vasu B, Bég OA, Gorla RS, Murthy PV. Magneto-bioconvection flow of a Casson thin film with nanoparticles over an unsteady stretching sheet: HAM and GDQ computation. International Journal of Numerical Methods for Heat & Fluid Flow. 2019.

[23] Zhang L, Arain MB, Bhatti MM, Zeeshan A, Hal-Sulami H. Effects of magnetic Reynolds number on swimming of gyrotactic microorganisms between rotating circular plates filled with nanofluids. Applied Mathematics and Mechanics. 2020;41(4):637-54.

[24] Shehzad SA, Reddy MG, Rauf A, Abbas Z. Bioconvection of Maxwell nanofluid under the influence of double diffusive Cattaneo–Christov theories over isolated rotating disk. Physica Scripta. 2020;95(4):045207.

[25] Khan NS, Shah Q, Bhaumik A, Kumam P, Thounthong P, Amiri I. Entropy generation in bioconvection nanofluid flow between two stretchable rotating disks. Scientific reports. 2020;10(1):1-26.

[26] Lin SP, Hsieh SC, Chen KI, Demirci A, Cheng KC. Semi-continuous bacterial cellulose production in a rotating disk bioreactor and its materials properties analysis. Cellulose. 2014;21(1):835-44.

[27] Magnacca G, Laurenti E, Vigna E, Franzoso F, Tomasso L, Montoneri E, Boffa V. Refuse derived bio-organics and immobilized soybean peroxidase for green chemical technology. Process Biochemistry. 2012;47(12):2025-31.

[28] Sarkar S, Roy D, Mukherjee J. Production of a potentially novel antimicrobial compound by a biofilm-forming marine Streptomyces sp. in a niche-mimic rotating disk bioreactor. Bioprocess and biosystems engineering. 2010;33(2):207-17.

[29] Chtioui O, Dimitrov K, Gancel F, Dhulster P, Nikov I. Rotating discs bioreactor, a new tool for lipopeptides production. Process Biochemistry. 2012;47(12):2020-4.

[30] Nikolov L, Karamanev D, Mamatarkova V, Mehochev D, Dimitrov D. Properties of the biofilm of Thiobacillus ferrooxidans formed in rotating biological contactor. Biochemical Engineering Journal. 2002;12(1):43-8.

[31] Bég OA, Kabir MN, Uddin MJ, Izani Md Ismail A, Alginahi YM. Numerical investigation of Von Karman swirling bioconvective nanofluid transport from a rotating disk in a porous medium with Stefan blowing and anisotropic slip effects. Proceedings of the Institution of Mechanical Engineers, Part C: Journal of Mechanical Engineering Science. 2020:0954406220973061.

[32] Anwar Bég O. Nonlinear multiphysical laminar nanofluid bioconvection flows: Models and computation. Computational approaches in biomedical nano-engineering. 2018:113-45.

[33] Chen KJ, Chen YS. Intensified production of biodiesel using a spinning disk reactor. Chemical Engineering and Processing: Process Intensification. 2014;78:67-72.

[34] Shamshuddin MD, Mishra SR, Kadir A, Bég OA. Unsteady chemo-tribological squeezing flow of magnetized bioconvection lubricants: numerical study. Journal of Nanofluids. 2019;8(2):407-19.

[35] Aranda JA. *Radiative heat transfer analysis of railroad bearings for wayside thermal detector optimization* (Doctoral dissertation, University of Texas Rio Grande Valley) 2018.

[36] Turkyilmazoglu, M. (2016). Natural convective flow of nanofluids past a radiative and impulsive vertical plate. *Journal of Aerospace Engineering*, *29*(6), 04016049.

[37] Shamshuddin MD, Khan SU, Bég OA, Beg TA. Hall current, viscous and Joule heating effects on steady radiative 2-D magneto-power-law polymer dynamics from an exponentially stretching sheet with power-law slip velocity: a numerical study. Thermal Science and Engineering Progress. 2020;20:100732.

[38] Khan BM, Gaffar SA, Beg OA. Entropy generation in magnetohydrodynamic radiative non-Newtonian dissipative convection flow from an inclined plane: numerical study. Nanoscience and Technology: An International Journal. 2020;11(4).

[40] Bég OA, Rashidi MM, Rastegari MT, Bég TA, Motsa SS, Halim A. DTM-Padé numerical simulation of electrohydrodynamic ion drag medical pumps with electrical Hartmann and electrical Reynolds number effects. Journal of Advanced Biotechnology and Bioengineering. 2013;1(2):62-79.

[41] Tripathi D, Bég OA, Gupta PK, Radhakrishnamacharya G, Mazumdar J. DTM simulation of peristaltic viscoelastic biofluid flow in asymmetric porous media: a digestive transport model. Journal of Bionic Engineering. 2015;12(4):643-55.

[42] Kumar M, Reddy GJ, Kumar NN, Bég OA. Application of differential transform method to unsteady free convective heat transfer of a couple stress fluid over a stretching sheet. Heat Transfer—Asian Research. 2019;48(2):582-600.

[43] Bhatti MM, Ullah Khan S, Anwar Bég O, Kadir A. Differential transform solution for Hall and ion-slip effects on radiative-convective Casson flow from a stretching sheet with convective heating. Heat Transfer. 2020; 49(2):872-88.

[44] Anwar Bég O, Kuharat S, Bég TA, Kadir A, Leonard HJ, Jouri WS. Computation of radiative heat transfer in solar direct absorber collector flows with robust numerical methods and multi-physical effects.,

"Understanding Thermal Radiation", chapter 3, pp. 100-205, Ed. K.S. Rawat, Nova Science, New York, June (2021). **In press**

[45] Anwar Bég O, Jouri WS, Bég TA, Kadir A, Leonard HJ, Shamshuddin MD, Hung TK. Computation of asymmetric micropolar squeezing flow in a bionic prosthetic dual disk system with blowing (injection) and Reynolds number effects, *Int. Conf. Advances in Mathematics, Physics & Applied Science (ICAMPA), New Delhi, India, March 1st (2020).*

[46] Siddiqui, A. A., & Turkyilmazoglu, M. (2019). A new theoretical approach of wall transpiration in the cavity flow of the ferrofluids. *Micromachines*, *10*(6), 373.

[47] Turkyilmazoglu, M. (2021). On the transparent effects of Buongiorno nanofluid model on heat and mass transfer. *The European Physical Journal Plus*, *136*(4), 1-15.

[48] Siddiqui, A. A., & Turkyilmazoglu, M. (2020). Natural convection in the ferrofluid enclosed in a porous and permeable cavity. *International Communications in Heat and Mass Transfer*, *113*, 104499.